

# Electron-molecule scattering calculations in a 3D finite element *R*-matrix approach

Stefano Tonzani

*JILA, University of Colorado, Boulder, Colorado 80309-0440*

Chris H. Greene

*Department of Physics and JILA, University of Colorado, Boulder, Colorado 80309-0440*

(Dated: November 17, 2018)

## Abstract

We have implemented a three-dimensional finite element approach, based on tricubic polynomials in spherical coordinates, which solves the Schrödinger equation for scattering of a low energy electron from a molecule, approximating the electron exchange as a local potential. The potential is treated as a sum of three terms: electrostatic, exchange and polarization. The electrostatic term can be extracted directly from *ab initio* codes (GAUSSIAN 98 in the work described here), while the exchange term is approximated using different local density functionals. A local polarization potential approximately describes the long range attraction to the molecular target induced by the scattering electron.

PACS numbers: 34.80.-i

## I. INTRODUCTION

Electron-molecule processes are important in many different areas of physics and chemistry, for instance in cold plasmas (that are present in interstellar media [1] and the high atmospheric layers). They are also relevant in radiation damage to living tissue, [2] and in surface physics and chemistry for example in electron-beam induced chemistry. [3] Theoretical studies of electron collisions with molecular targets have been carried out since the late 1970s (see for example Refs. 4, 5, while Ref. 6 presents an extensive review of the state of the field up to the early 1980s). Some of the adopted techniques include the Kohn variational principle, [7] the Schwinger variational principle [8] and the *R*-matrix method [9] used in this study. These methods have proven capable of describing scattering from increasingly complex molecular targets. [10, 11]

The need for a simple but general method to deal with electron scattering by a polyatomic target, that does not utilize single center expansions or Gaussian basis functions has led us to develop a new approach. Much of our motivation derives from our goal of describing dissociative recombination reactions and the role of Rydberg states in these processes. Each of the techniques that constitute our method has been widely used in the past, including the use of finite elements in scattering processes, [12, 13] and the introduction of model potentials to describe electron scattering. [4, 5] Nevertheless, to our knowledge, this is the first attempt to combine a three dimensional finite element calculation with the *R*-matrix method. We hope that this approach can be used to calculate quantum defect parameters, which can in turn describe vibrational-electronic coupling in polyatomic molecules through an implementation of quantum defect theory (QDT) techniques.[14, 15, 16, 17]

For this pilot study we describe the electron-molecule interaction through an indepen-

dent particle picture. There are three main sources of interaction between a low-energy electron and a closed shell molecule: the direct electrostatic interaction, which is always the largest contribution to the potential, the exchange interaction, which makes the potential nonlocal and derives from the antisymmetrization of the wavefunction, and a correlation and polarization term that describes the response of the target to the continuum electron. The polarization term is dealt with using a simple long range polarization potential.

The exchange term, due to its nonlocality, is the most complicated to model. We reduce it to a local potential by adopting the widely employed local density approximation (LDA). While this is a rather crude approximation to this term in the potential, it is well-known that it gives surprisingly realistic results; moreover it enables us to reduce the solution of the complicated scattering of an electron from a multielectronic target to the solution of an effective one-body Schrödinger equation with a local potential. This description is expected to be realistic only for closed-shell molecular targets.

Finite element techniques are well established as flexible tools to solve partial differential equations in different fields of physics, and in engineering. [18]

Their introduction to quantum mechanical calculations dates back to the work of Shertzer and Botero, [12] who solved the scattering equations as a few-body problem. They have also been implemented in a study of two-electron photoejection from atoms. [19] A study that is closer in spirit to ours is the one by Weatherford, *et. al.* [13] which treats a simplified model Hamiltonian in a system possessing cylindrical symmetry, reducing the calculation to just two dimensions. The paper of Huo *et. al.* [20] uses instead an exact representation of the exchange potential, using a Gaussian basis set at short distance, and adopts finite elements only for the radial coordinate.

## II. THEORY

### A. Electron scattering equations

The electron molecule scattering problem, begins with the full Hamiltonian of the system:

$$\hat{H} = -\frac{1}{2} \sum_i \nabla_{r_i}^2 - \frac{1}{2} \sum_{\alpha} \nabla_{R_{\alpha}}^2 - \sum_{i,\alpha} \frac{Z_{\alpha}}{|\vec{r}_i - \vec{R}_{\alpha}|} + \sum_{\alpha > \beta} \frac{Z_{\alpha}Z_{\beta}}{|\vec{R}_{\alpha} - \vec{R}_{\beta}|} + \sum_{j > l} \frac{1}{|\vec{r}_j - \vec{r}_l|}. \quad (1)$$

This operator contains both the nuclear and electronic degrees of freedom, indicated respectively with Greek and Latin indices. We treat here the electronic problem alone, within the Born-Oppenheimer approximation, namely freezing the nuclei in some definite configuration (usually the equilibrium configuration) while solving for the electronic wavefunction. The treatment of vibrations can be carried out by repeating the electronic calculations for different values of the nuclear positions, followed by vibrational averaging or a vibrational frame transformation description. [21, 22] It is now possible to write a wavefunction that depends parametrically on the nuclear coordinates as an antisymmetrized product of the target and scattering electron wavefunctions:

$$\Psi_{\gamma} = \mathcal{A} \sum_{\gamma'} \Phi_{\gamma'}(\bar{i}, R) \phi_{0,\gamma'}(r_i) \quad (2)$$

where  $\gamma$  represents the set of quantum numbers that fully describe the state of the system, and the sum over  $\gamma'$  allows for different configurations of the compound system (target + scattered electron) to contribute. In Eq. 2  $\bar{i}$  represents the coordinates of all the electrons except the  $i$ -th.

If only the ground state configuration  $\gamma'$  in this sum is retained, the approximation made

is called static exchange. It is possible to show [23] in this case that the  $(N + 1)$ -particle Schrödinger equation can be reduced to  $N + 1$  single particle equations for the individual orbitals. We are interested in the orbital  $\phi_0$  for the scattered electron, which obeys

$$(-\nabla^2 + V_s - E)\phi_0(\vec{r}) = \sum_{j=1}^N \phi_j(\vec{r}) \int d\vec{r}' \frac{\phi_j^*(\vec{r}')\phi_0(\vec{r}')}{|\vec{r} - \vec{r}'|} \quad (3)$$

where the  $\phi_j$  ( $j \geq 1$ ) are the target molecular orbitals. The electrostatic potential  $V_s$  is the averaged Coulomb interaction of the scattered electron with all the other electrons and the nuclei

$$V_s(\vec{r}) = \sum_{j=1}^N \int d\vec{r}' \frac{\phi_j^*(\vec{r}')\phi_j(\vec{r}')}{|\vec{r} - \vec{r}'|} - \sum_{\alpha} \frac{Z_{\alpha}}{|\vec{r} - \vec{R}_{\alpha}|}. \quad (4)$$

The term on the right hand side of Eq. 3 is referred to as exchange potential.

## B. *R*-matrix method

The *R*-matrix method is a well-established tool for problems where the continuum portion of the spectrum of a Hamiltonian must be treated. In its usual implementation, it involves diagonalization of the (Bloch-modified) Hamiltonian operator in a box subject to some fixed boundary condition obeyed by the basis orbitals. The *R*-matrix box partitions the space in two, with an internal reaction zone, to which all the short-range interactions are confined, and an external zone, where instead either no potential is present or there is a long range Coulomb or dipole potential (or both), and the behavior of the solutions of the Schrödinger equation is very simple. In some studies, other long-range multipole potentials are included in the external zone. [24, 25] We use the *R*-matrix method in the eigenchannel form.[26] In this case we seek those stationary states for which the logarithmic derivative of the

wavefunction at the surface of the  $R$ -matrix box is constant at every point. Refs. 27, 28, 29 derive a new variational principle,

$$b \equiv -\frac{\partial \log(r\Psi_\beta)}{\partial r} = 2 \frac{\int_V \Psi^*(E - \hat{H} - \hat{L})\Psi dV}{\int_V \Psi^* \delta(r - r_0) \Psi dV}, \quad (5)$$

for the logarithmic derivative of the wavefunction. If  $\Psi$  is discretized in some basis set inside a spherical box, within which all the short range dynamics is localized, this results in a generalized eigenvalue problem for  $b$ :

$$\underline{\Gamma} \vec{C} = (E - \underline{H} - \underline{L}) \vec{C} = \underline{\Lambda} \vec{C} b \quad (6)$$

where  $\underline{\Lambda}$  is the overlap of the basis functions calculated on the surface of the  $R$ -matrix box and  $\hat{L}$  is the Bloch operator, defined as

$$\hat{L} = \frac{1}{2} \delta(r - r_0) \frac{\partial}{\partial r} r \quad (7)$$

and  $r_0$  is the radius of the box. The eigenvector  $\vec{C}$  represents the expansion coefficients of the basis set used. Both  $\underline{\Gamma}$  and  $\underline{\Lambda}$  are defined in the appendix for the finite element basis set used in this work. It is possible to partition the basis functions in two subspaces, closed and open, depending on whether their value at the surface of the box is zero or nonzero. [26] This allows us to reduce the burden of the solution of Eq. 6 to the easier task of solving a much smaller eigenvalue problem of type

$$\Omega \vec{C}_o = (\underline{\Gamma}_{oo} - \underline{\Gamma}_{oc} \underline{\Gamma}_{cc}^{-1} \underline{\Gamma}_{co}) \vec{C}_o = \underline{\Lambda}_{oo} \vec{C}_o b \quad (8)$$

in the open functions subspace, in addition to the large auxiliary system of equations:

$$\underline{\Gamma}_{cc}\vec{C}_c = -\underline{\Gamma}_{co}\vec{C}_o \quad (9)$$

where the subscripts indicate the matrix blocks. At the boundary of the  $R$ -matrix box  $\Psi$  is matched to an external solution depending on the long range tail of the potential (Bessel functions for neutral molecules, Coulomb functions for molecular ions). This allows us to calculate the reaction matrix  $\underline{K}$ , from which the scattering matrix is derived as

$$\underline{S} = \frac{1 + i\underline{K}}{1 - i\underline{K}} \quad (10)$$

Scattering cross sections can then be calculated in the standard manner.

### C. Finite element method

The essence of the finite element method is the use of a basis set that is defined over small local regions. By this we mean that each basis function is nonzero only within a small region, and it has a simple polynomial form. By using many “sectors” or “elements” (the volume over which the local basis function is defined) though, it is possible to reproduce very complex features of the solutions to the differential equation of interest. We discretize  $\Psi$  using finite element polynomials in all three dimensions. The basis set is a direct product of 4 cubic Hermite polynomials defined locally in each sector for each dimension. The use of a spherical coordinate grid, in  $r, \theta, \phi$  makes the boundaries of the sectors simple and the three-dimensional integrals (the main bottleneck of these calculations) faster to calculate.

The finite element basis set is composed of piecewise polynomials, which provides ad-

vantages over a global variable representation. In particular one can treat potentials and wavefunctions of complicated form by simply reducing the size of the elements in which the polynomials are defined, in those areas where fine features arise. In our case the basis functions are third order Hermite polynomials, which allow us to achieve function and derivative continuity, while still permitting a simpler implementation compared to higher order polynomials. Each polynomial is defined in a hexahedral sector (a cube in the rescaled variables used for the evaluation of the integrals), and since the wavefunction is discretized in terms of finite elements in all three dimensions, the basis set is a direct product of 4 polynomials in each dimension per sector, which means 64 basis functions are defined in each sector.

In finite element analysis (FEA) the polynomials are matched with the ones in neighboring sectors to ensure functional and derivative continuity (and mixed derivative continuity also, in multidimensional FEA). Each sector has 8 physical nodes (at the edges of the cube) and the basis functions defined in the sector have coefficients (to be determined by the solution of the Schrödinger equation) that represent the value of the wavefunction, or its derivatives, at the nodal point. In the language of finite element analysis, a node is the vertex of one of the sectors into which the three-dimensional space is divided. The matching at the boundary of each sector is imposed when assembling the global Hamiltonian matrix from the local ones. The global index of functions that correspond to the same node and quantity (e. g. derivative) in neighboring sectors has to be the same. Their matrix elements have hence to be summed together. Details of the procedure are given in the appendix.

#### D. Local Density Approximation (LDA)

Using an approach derived from Refs. 4, 5, we approximate the exchange integral (that is nonlocal), by a local form using free electron gas (FEG) orbitals, [30] i.e. plane waves, for

the target molecule and using the first order Born approximation

$$\phi_0 = Ne^{i\vec{k}\cdot\vec{r}} \quad (11)$$

for the scattered electron. The arbitrary normalization constant  $N$  is unimportant and it disappears as soon as we express the exchange functional as a product of a local exchange potential times the scattered wave. After these substitutions are made, it is possible to evaluate the integral on the right hand side of Eq. 3 analytically, obtaining a local potential of the form

$$V_{ex}(\vec{r}) = -\frac{2}{\pi}k_F F(\eta), \quad (12)$$

whereas the Fermi momentum  $k_F$  (the momentum of the electron that is at the top of the Fermi sea in a free electron gas) is:

$$k_F(\vec{r}) = (3\pi^2\rho(\vec{r}))^{1/3}. \quad (13)$$

The other functions present in Eq. 12 are

$$F(\eta) = \frac{1}{2} + \frac{1-\eta^2}{4\eta} \log \left| \frac{1+\eta}{1-\eta} \right| \quad (14)$$

$$\eta = \frac{k}{k_F}, \quad (15)$$

where  $k$  is the modulus of the momentum of the scattered electron. It should be noticed that the exchange potential in Eq. 12 is energy dependent.

Many functionals of this form exist, [4] with minor differences in the expression for  $k$ , the scattering electron wavenumber. The functional we have used most successfully is the Hara

exchange [31] where

$$k = \sqrt{2(E + I) + k_F^2} \quad (16)$$

and  $I$  is the ionization energy of the molecule while  $E$  is the energy of the incident electron, this emerges from the assumption that the scattered electron and the electron in the highest energy bound state (the Fermi electron, which has momentum  $k_F$ ) move in the same potential field;  $V_{ex}$  then depends only on  $\vec{r}$ , through the electron density  $\rho(\vec{r})$ , as a local potential, and on the energy, through the functional dependence of the momentum  $k$  as approximated in Eq. 16.

We have also experimented with other functional forms of the exchange interaction (still based on a FEG approximation). One in particular is the Slater exchange, [23] derived by averaging the function  $F(\eta)$  over the momenta of all the electrons up to the Fermi level, which has often been used to calculate bound states in atoms and molecules. However the results using Slater exchange are unsatisfactory, presumably owing to the neglect of the energy dependence in this model.

Since our main goal is to treat low energy scattering processes (0-10 eV) we linearize the energy dependence of the functional in Eq. 14, in order to calculate the exchange potential matrix elements at all energies at once. For a molecule like CO<sub>2</sub>, the matrix element calculation requires around 2 hours on an Alpha 500 Mhz workstation. The next step is the solution of the linear system and the determination of the scattering observables, which requires approximately 15 minutes per energy desired, for a basis set size of 33000. This step is trivially parallelizable, of course. The results improve upon inclusion of a

polarization potential

$$V_{pol} = -\frac{1}{2r^4}(\alpha_0 + \alpha_2 P_2(\cos \theta))(1 - e^{-(\frac{r}{r_c})^6}) \quad (17)$$

where  $r_c$  is a distance parameter comparable to the range of the target charge distribution. When high accuracy is needed for resonance positions in some applications,  $r_c$  can be determined empirically [4] to reproduce the energies of one or more resonances of interest.

All the information needed to construct the potential matrix can be extracted from standard *ab initio* quantum chemistry codes; in this work we have used GAUSSIAN 98. The electrostatic potential and the electronic density (needed to construct the exchange functional) for the target molecule are calculated on a uniform cubic grid at a CI (singles and doubles) level for the molecules presented here. The difference in using an electrostatic potential and density calculated at the RHF level or at the CI level for CO<sub>2</sub> at its equilibrium geometry amounts roughly to a difference of 10% in the calculated phase shifts and overall magnitude of the elastic cross sections. These calculations usually require a minimal amount of time, of the order of ten minutes per nuclear geometry for CO<sub>2</sub> on the aforementioned computational platform. The potentials are then interpolated on the three-dimensional quadrature grid using fifth order splines.

## E. Computational Details

The three-dimensional integrals, as was mentioned above, are the bottleneck of the entire procedure, making it highly desirable to minimize the time spent in their calculation. For the sectors that do not contain a nucleus it is possible to use just 4 Gauss-Legendre points of integration, since doubling the number of points changes the calculated phase shifts by only

about  $10^{-6}$  radians, while increasing the computational time by approximately an order of magnitude. Particular caution has to be observed when integrating over sectors that contain a nucleus. We have found it important in general to have a finite element vertex on the Coulomb singularity, in order to obtain correct results, and to use more integration points. In these sectors we use 20 integration points in each dimension since we found that the convergence of the phase shifts in this case is, as in the previous case, about  $10^{-6}$ .

The sparse structure of the finite element matrices (see Fig. 8) can be exploited with great advantage from the beginning. No matter how the grid is defined, each basis function has matrix elements with at most 216 functions. This allows us to know the data structure of the matrix  $\Gamma$  in Eq. 6 in advance and store just the nonzero elements, with a reduction of memory cost of approximately two orders of magnitude. This economy is crucial to allow us to perform three dimensional calculations in the first place.

The dimension  $N$  of the eigensystem in Eq. 6 is, for  $\text{CO}_2$ , of the order of 40000, whereas for the open subspace it is only 100 or less.  $N$  increases rapidly with the complexity and spatial extension of the molecular potential, but the sparsity of the matrices is high (about 0.5% full for  $N \sim 40000$ ), and it increases with the dimension of the system. Depending on  $N$  we use different techniques to solve the linear system in Eq. 9 : for small  $N$  we use direct sparse LU factorization solvers (SuperLU); otherwise iterative biconjugate gradient methods are used. Different preconditioners have been tried in this context to speed up the solution of the linear system, the one we have found to work the best for us is an incomplete Choleski factorization, which reduces drastically the number of iterations with respect to a diagonal preconditioner, the  $\underline{\Gamma}$  matrix in Eq. 9 is not, in fact, diagonally dominant. Clearly, the degree to which the factorization is carried out influences its nonzero structure. The factorization is carried out to the extent that the original structure is preserved.

Iterative methods are slower than direct factorization, in the tests we have performed normally the direct method is faster by a factor of ten, but for large systems an iterative solver is essentially the only option, owing to memory limitations. Since the factorization of a sparse matrix does not preserve the sparsity pattern, the factorized matrices present storage problems, since a fill-in factor of around 10 is common for these systems.

### III. RESULTS

#### A. Neutral molecules

We have tested our approach in calculations of electron scattering by  $\text{N}_2$  and  $\text{CO}_2$ , classic benchmarks in this field, [4, 32, 33] because their elastic cross sections exhibit striking features that can be challenging to reproduce. The strong and narrow  $\Pi_g$  resonance at 2.4 eV in  $\text{N}_2$  is reproduced in our calculations at the right energy, provided we use a physically reasonable cutoff radius  $r_c = 2.8$  a.u. for the polarization potential. The results are shown in Fig. 4. The resonance is reproduced also at the static exchange level (without using a long range polarization potential), but at an energy higher by approximately 1.5 eV.

For  $\text{CO}_2$  the main feature in the total elastic cross section is a  $\Pi_u$  resonance at 3.8 eV. To reproduce it at the correct energy we have to tune the polarization cutoff radius to 2.4 a.u.. This feature is present also at the static exchange level, at 8 eV. The dependence on the polarization, as one expects from the larger spatial extension, the larger number of electrons and the greater asymmetry of this molecule, becomes much more pronounced than in  $\text{N}_2$ . The scattering cross section for this system is shown in Fig. 3. The value of the cutoff radius for the polarizability potential, which is the only adjustable parameter in the model, is reasonable. This is clear from Fig. 2 which demonstrates that this potential is appreciable

just outside the region where the main part of the electronic density is located. The results are always in good agreement with previous theory, as shown in the figures. Vibrational effects tend to broaden these resonances in experimental elastic scattering cross sections, and they also give rise to more structured resonance peaks, which are not considered in this work. The present calculations have been performed for the molecular targets only at their equilibrium distances. The values of the polarizabilities used in these calculations are [4]  $\alpha_0 = 11.89a_0^3$  and  $\alpha_2 = 4.19a_0^3$  for  $\text{N}_2$  and [6]  $\alpha_0 = 17.9a_0^3$ ,  $\alpha_2 = 9.19a_0^3$  for  $\text{CO}_2$ . It should be pointed out that accurate static polarizability coefficients  $\alpha_0$  and  $\alpha_2$  in Eq. 17 can also be extracted from *ab initio* calculations. Generally, the low-lying shape resonances present in these small molecules are spatially highly localized, which allows the radius of the *R*-matrix box to be kept small, around 8 to 14 a.u. for the present calculations.

In the case of the third neutral molecule that we present here, ethylene, the situation is more complicated. Since the target is now nonlinear it is more difficult to describe it in a discrete basis set and it is more expensive computationally to calculate the scattering cross section. Nevertheless we are able to reproduce the features of the elastic cross section for this molecule. We find good agreement with the energies of the resonances and with the overall cross section magnitude, compared with previous theory and also experimental data, although the vibrational effects again tend to broaden the resonance peak.

It should be noticed parenthetically that if we neglect exchange altogether in calculations for all of the molecules presented here, the cross sections are qualitatively wrong, with resonances far lower in energy than the experimental ones and in the wrong symmetry channels. This is due to the fact that some of the target electrons are not bound anymore, because the static potential is not attractive enough. Once added, the exchange potential is basically an attractive local potential, resulting in the correct number of bound states for the

target; consequently the scattering resonances are generated by capture of the electron in truly unoccupied molecular orbitals of the target. A more systematic study of the behavior of the cross sections, when different parts of the potential are neglected altogether, can be found in Ref. 6.

## B. Quantum defect calculations

It has been shown [34] that use of a local density approximation can often be effective in calculating molecular quantum defects, for bound or scattering states, for small closed-shell target molecules. It is possible to calculate quantum defects from a scattering calculation carried out near zero energy. The key step is to diagonalize the  $K$ -matrix

$$K_{ii'} = \sum_{\alpha} U_{i\alpha} \tan \pi \mu_{\alpha} U_{\alpha i'}^T$$

and then utilize the relationship between the quantum defect and the scattering phase shift, [26, 35]

$$\delta_l = \pi \mu_l \quad (18)$$

Accordingly quantum defects can be extracted from electron-scattering calculations at positive or negative energies. These quantum defects can then be used to determine the Born-Oppenheimer potential curves of the Rydberg states converging to the various ionization thresholds through the Rydberg formula. [26] these can then be exploited through MQDT techniques, to extract dynamical information on, for example, dissociative recombination, [14] a process that we will study in the future using the machinery developed in this paper. Here we show an example of how well this approach works for a simple diatomic

molecule.

We compare our results to the work of Sarpal and Tennyson [36] which made no approximation about the nature of the electron-molecule potential. It is possible to see that the agreement is generally very good. The quantum defects represented in Fig. 6 are the most important ones, higher symmetries and partial waves ( $l > 2$ ) having very small phase shifts at the low energies considered here. In electron scattering from an ionic target we must account for the fact that heteronuclear molecules like HeH have a dipole moment, so we must transform from the center of mass frame to a new frame centered on the center of charge (the proton in this case). It is then possible to match to simple Coulomb functions at the boundary of the box. Otherwise multipole potentials have to be included in the external region.

#### IV. CONCLUSIONS

In this paper we have shown how a combination of the  $R$ -matrix method and a three-dimensional finite element basis set can provide a promising tool for solving problems in which a low-energy electron collides with a polyatomic molecule. It should be emphasized that to perform three-dimensional calculations in a local basis set there is need for special computational techniques, namely sparse matrix techniques. These calculations are in general very complicated and time consuming, so some approximation must be made in order to make them sufficiently manageable. In the present work we approximate the exchange term in the potential, which is nonlocal, as a local potential using the free electron gas approximation. The results are shown to be qualitatively accurate for a number of molecules even in this rather crude approximation. Nevertheless there is room for improvement for further work directed at treating exchange exactly and including relaxation of the target

orbitals in the presence of the scattering electron.

### Acknowledgments

This work was supported by the Department of Energy, Office of Science, and by an allocation of NERSC supercomputing resources. We thank J. Shertzer for useful discussions at an early stage of the project. We have also benefited from a number of useful discussions with R. Santra.

### APPENDIX A: FINITE ELEMENT MATRICES

Starting from Eq. 6 we define the matrices  $\Gamma$  and  $\Lambda$  in our finite element basis transforming first to spherical coordinates (the box is spherical and the grid is also defined in spherical coordinates), and then to rescaled coordinates, which are the variables of the local polynomials. In the rescaled variables each sector is transformed to a cube, in which the range of each variable is from 0 to 1. The nodal structure of each element is represented in Fig. 7 and the wavefunction inside each sector can be expanded as

$$u(\xi_1, \xi_2, \xi_3) = \sum_{i,j,k,l,m,n} \psi_i^l(\xi_1) \psi_j^m(\xi_2) \psi_k^n(\xi_3) C_{node}^{(lmn)} \quad (A1)$$

where  $i, j, k$  can be 1 if the polynomial has nonzero value at some node or 2 if it has nonzero derivative, whereas  $l, m, n$  can assume values of 0 if that node is the first for the variable of the polynomial in the sector or 1 if it is the last;  $\xi_i$  are the local rescaled variables. The coefficients  $C_{node}^{(lmn)}$  are the values of the wavefunction and its derivatives at the node, and

they are to be determined solving Eq. 6. If we define

$$a_{k,p} = x_{k,p,i+1} - x_{k,p,i} \quad (\text{A2})$$

$$x_{k,p} = a_{k,p} \xi_k + x_{k,p,i} \quad (\text{A3})$$

where  $k$  indexes the spherical coordinates and  $p$  the sectors in which they are defined,  $x_{k,p,i}$  and  $x_{k,p,i+1}$  are the initial and final points for the variable  $x_k$  in sector  $p$ , the expressions for the matrices become:

$$\Gamma_{ij} = \int \left[ \sum_k^3 \frac{F(x_k)}{a_k a_k} \frac{\partial u_i}{\partial \xi_k} \frac{\partial u_j}{\partial \xi_k} + 2u_i(U - E)u_j \right] a_r a_\theta a_\phi r^2 \sin^2 \theta d\xi_1 d\xi_2 d\xi_3 \quad (\text{A4})$$

$$\Lambda_{mn} = \int Y_{lm}^*(\theta, \phi) Y_{l'm'}(\theta, \phi) \sin \theta \, d\theta \, d\phi = \delta_{ll'} \delta_{mm'} \quad (\text{A5})$$

where  $F(x_k)$  is a spherical coordinates scale factor, and it is 1 if  $x_k = r$  and  $1/r^2$  and  $1/(r^2 \sin^2 \theta)$  for  $\theta$  and  $\phi$  respectively. Imposing function and derivative continuity for  $u(\xi_1, \xi_2, \xi_3)$  amounts to require that the indices of the same node across neighboring sectors be the same. This in turn leads to having to perform a sum of the integrals in Eq. A4 when evaluating the matrix element at a node, across all sectors that share that node.

---

[1] B. J. McCall and T. Oka, *Science* **287**, 1941 (2000).

[2] B. Boudaïffa, P. Cloutier, D. Hunting, M. A. Huels, and L. Sanche, *Science* **287**, 1658 (2000).

[3] R. Balog and E. Illenberger, *Phys. Rev. Lett.* **91**, 213201 (2003).

[4] M. Morrison and L. A. Collins, *Phys. Rev. A* **17**, 918 (1978).

[5] D. Dill and J. L. Dehmer, *Phys. Rev. A* **21**, 85 (1980).

- [6] N. F. Lane, Rev. Mod. Phys. **52**, 29 (1980).
- [7] B. I. Schneider and T. N. Rescigno, Phys. Rev. A **37**, 3749 (1988).
- [8] D. K. Watson, R. R. Lucchese, V. McKoy, and T. N. Rescigno, Phys. Rev. A **21**, 738 (1980).
- [9] J. Tennyson, C. J. Noble, and S. Salvini, J. Phys. B **17**, 905 (1984).
- [10] F. A. Gianturco and R. R. Lucchese, J. Chem. Phys. **114**, 3429 (2001).
- [11] R. R. Lucchese, F. A. Gianturco, and N. Sanna, Chem. Phys. Lett. **305**, 413 (1999).
- [12] J. Shertzer and J. Botero, Phys. Rev. A **49**, 3673 (1994).
- [13] C. A. Weatherford, M. Dong, and B. C. Saha, Int. J. Quant. Chem. **65**, 591 (1997).
- [14] V. Kokouoline and C. H. Greene, Phys. Rev. A **68**, 012703 (2003).
- [15] N. A. Harris and C. Jungen, Phys. Rev. Lett. **70**, 2549 (1993).
- [16] S. L. Guberman and A. Giusti-Suzor, J. Chem. Phys. **95**, 2602 (1991).
- [17] H. Takagi, in *Dissociative Recombination of Molecular Ions With electrons*, edited by S. L. Guberman (Kluwer Academic / Plenum Publishers, New York, 2003), p. 177.
- [18] K. J. Bathe, *Finite Element Procedures* (Prentice-Hall, Englewood Cliffs, N. J., 1996).
- [19] K. W. Meyer, C. H. Greene, and B. D. Esry, Phys. Rev. Lett. **78**, 4902 (1997).
- [20] W. M. Huo and D. Brown, Phys. Rev. A **60**, 295 (1999).
- [21] C. Greene and C. Jungen, Adv. Atom. Mol. Phys. **21**, 51 (1985).
- [22] U. Fano, J. Opt. Soc. Am. **65**, 979 (1975).
- [23] J. C. Slater, *Quantum Theory of Molecules and Solids*, vol. IV (McGraw-Hill, New York, 1974).
- [24] B. D. Esry, C. H. Greene, and J. P. Burke, Jr., Phys. Rev. Lett. **83**, 1751 (1999).
- [25] N. R. Badnell and M. J. Seaton, J. Phys. B **32**, 3955 (1999).
- [26] C. H. Greene, M. Aymar, and E. Luc-Koenig, Rev. Mod. Phys. **68**, 1015 (1996).

[27] C. H. Greene, in *Fundamental Processes of Atomic Dynamics*, edited by J. Briggs, H. Kleinpoppen, and H. Lutz (Plenum, New York, 1988).

[28] H. LeRouzo and G. Raseev, Phys. Rev. A **29**, 1214 (1984).

[29] U. Fano and C. M. Lee, Phys. Rev. Lett. **31**, 1573 (1973).

[30] W. Kohn and L. J. Sham, Phys. Rev. **140**, A1133 (1965).

[31] S. Hara, J. Phys. Soc. Jpn. **27**, 1009 (1969).

[32] M. G. Lynch, D. Dill, J. Siegel, and J. L. Dehmer, J. Chem. Phys. **71**, 4249 (1979).

[33] T. N. Rescigno, D. A. Byrum, W. A. Isaacs, and C. W. McCurdy, Phys. Rev. A **60**, 2186 (1999).

[34] M. Tashiro and S. Kato, J. Chem. Phys. **117**, 2053 (2002).

[35] M. J. Seaton, Rep. Prog. Phys. **46**, 167 (1983).

[36] B. K. Sarpal and J. Tennyson, J. Phys. B **25**, L49 (1992).

[37] C. Szmytkowski, A. Zecca, G. Karwasz, S. Oss, K. Maciag, B. Marinkovic, R. S. Brusa, and R. Grisenti, J. Phys. B **20**, 5817 (1987).

[38] C. Winstead, P. Hipes, M. A. P. Lima, and V. McKoy, J. Chem. Phys. **94**, 5455 (1991).

[39] B. I. Schneider, T. N. Rescigno, B. H. Lengsfield, and C. W. McCurdy, Phys. Rev. Lett. **66**, 2728 (1991).

[40] R. Panajotovic, M. Kitajima, H. Tanaka, M. Jelisavcic, J. Lower, L. Campbell, M. J. Brunger, and S. J. Buckman, J. Phys. B **36**, 1615 (2003).

[41] O. Sueoka and S. Mori, J. Phys. B **19**, 4035 (1986).

## FIGURES

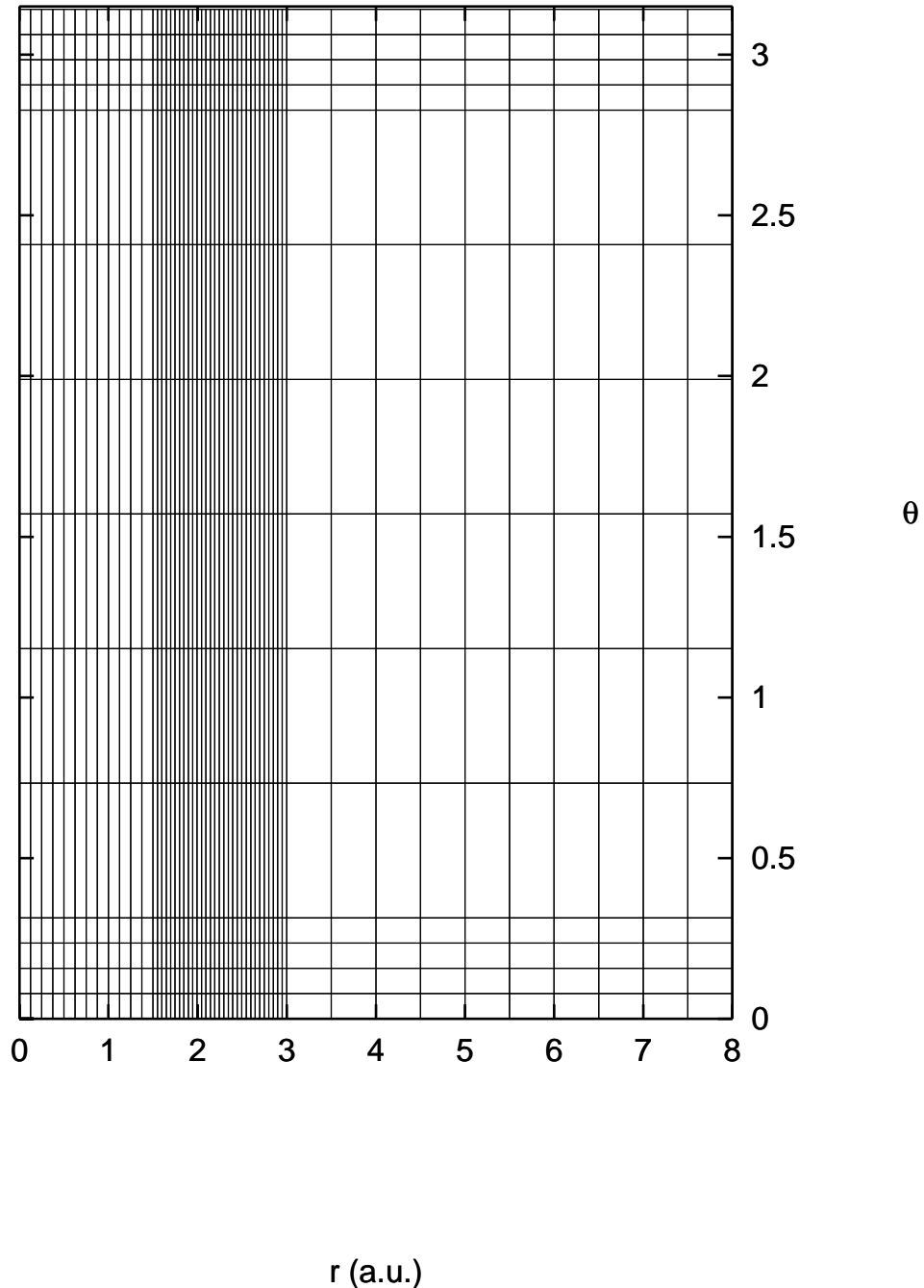


FIG. 1: From this two dimensional cut in the radius  $r$  and the polar angle  $\theta$  of the finite element grid (for a  $\text{CO}_2$  target), it is possible to notice the finer mesh near the oxygen nuclei localized at  $r = 2.19$  a.u. and  $\theta = 0$  and  $\pi$  respectively, while the carbon is located at the center of the grid.

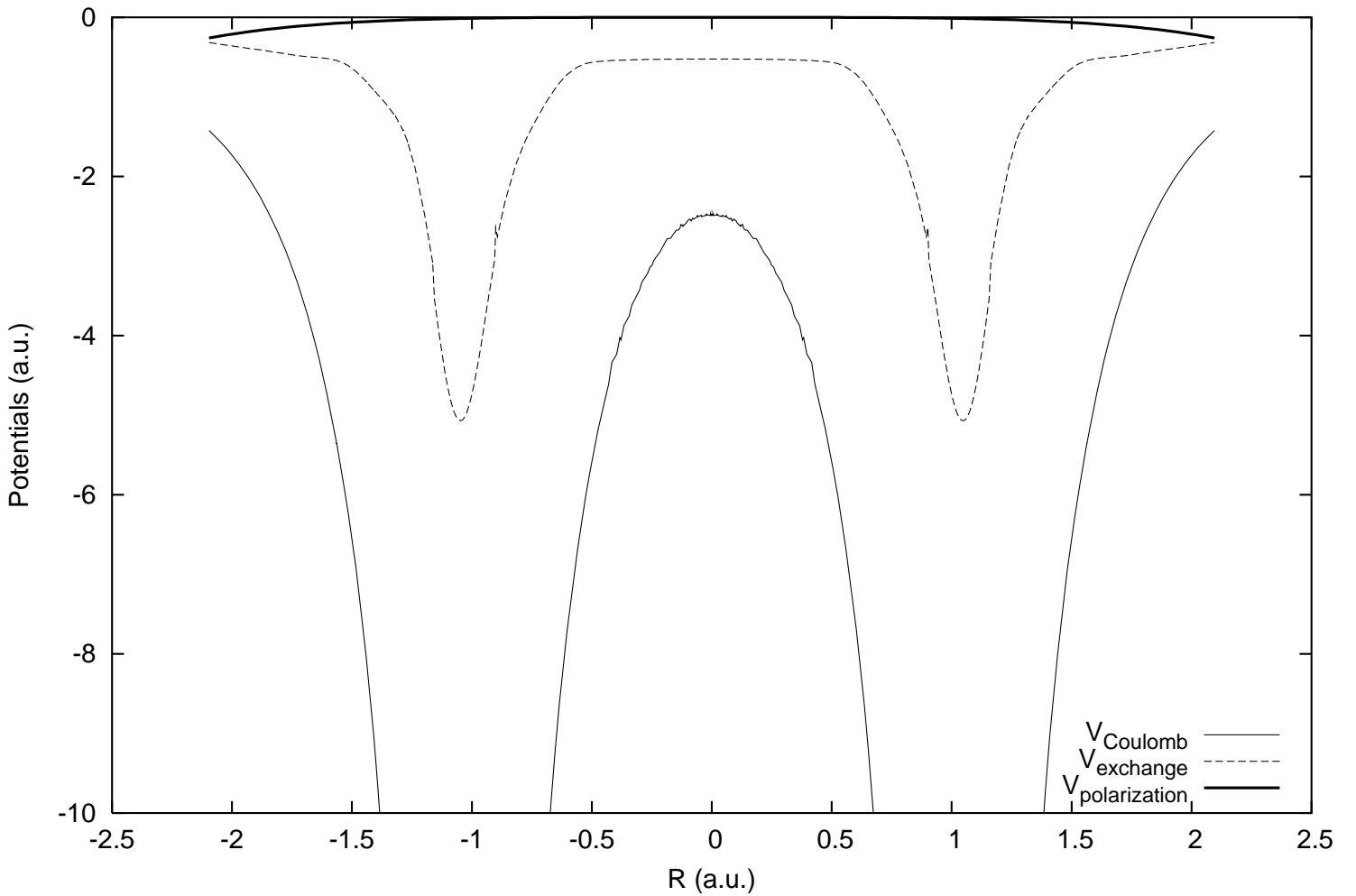


FIG. 2: The three terms of the potential for a  $\text{N}_2$  molecule. The exchange potential is large only at the nuclei (at  $r = -1.094$  and  $r = 1.094$  a.u. in the equilibrium configuration of the molecule) where the static potential is singular, so  $V_{\text{ex}}$  is always much smaller than  $V_s$ . On the other hand the polarization potential becomes important in the outer zone, where the electron density of the molecule goes to zero.

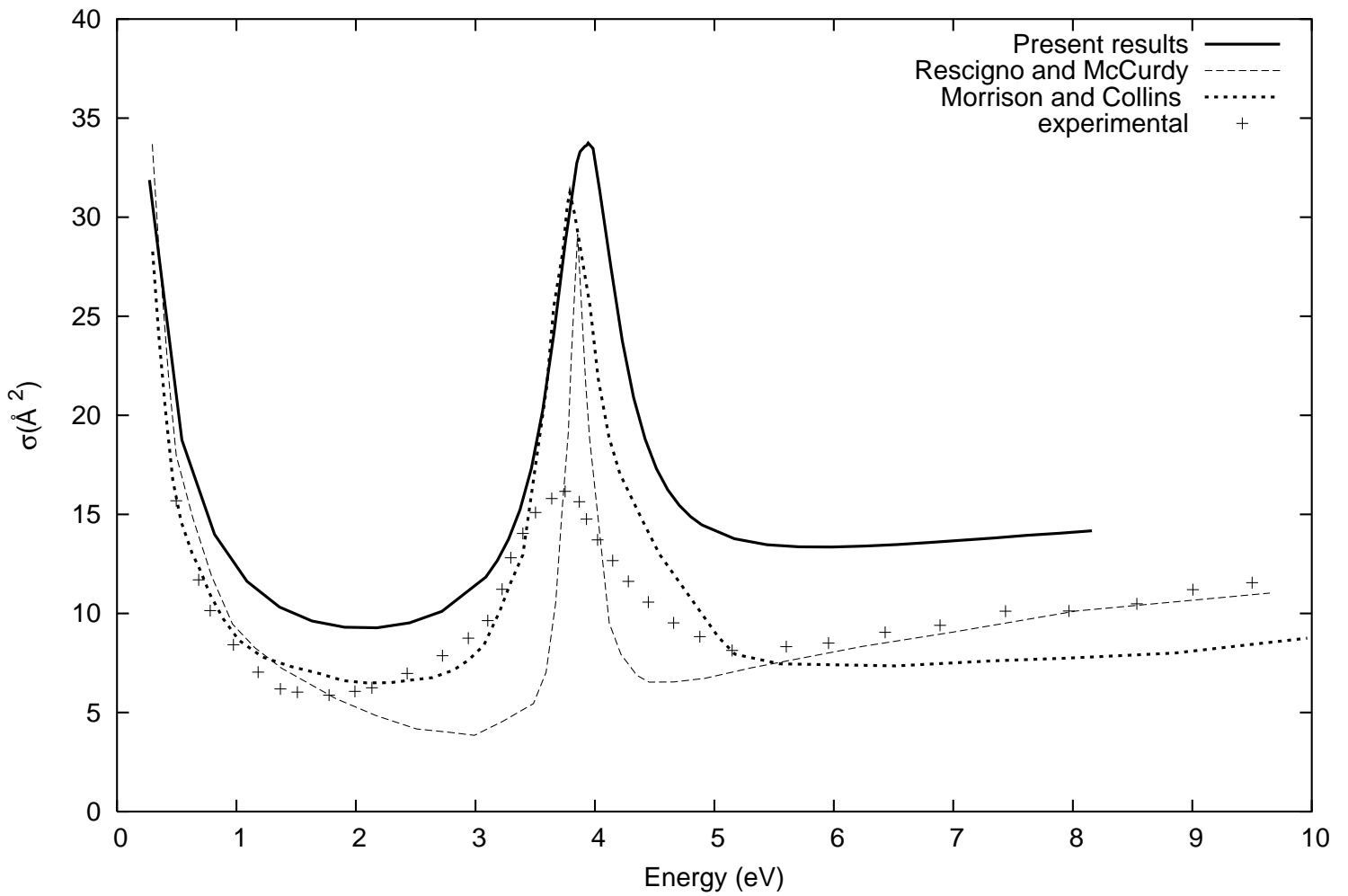


FIG. 3: Total elastic cross section for scattering of electrons from  $\text{CO}_2$ . The present results are compared with previous theory from Rescigno *et al.* [33] and Morrison and Lane, [6] whereas the experimental results are those of Szmytkowski. [37]

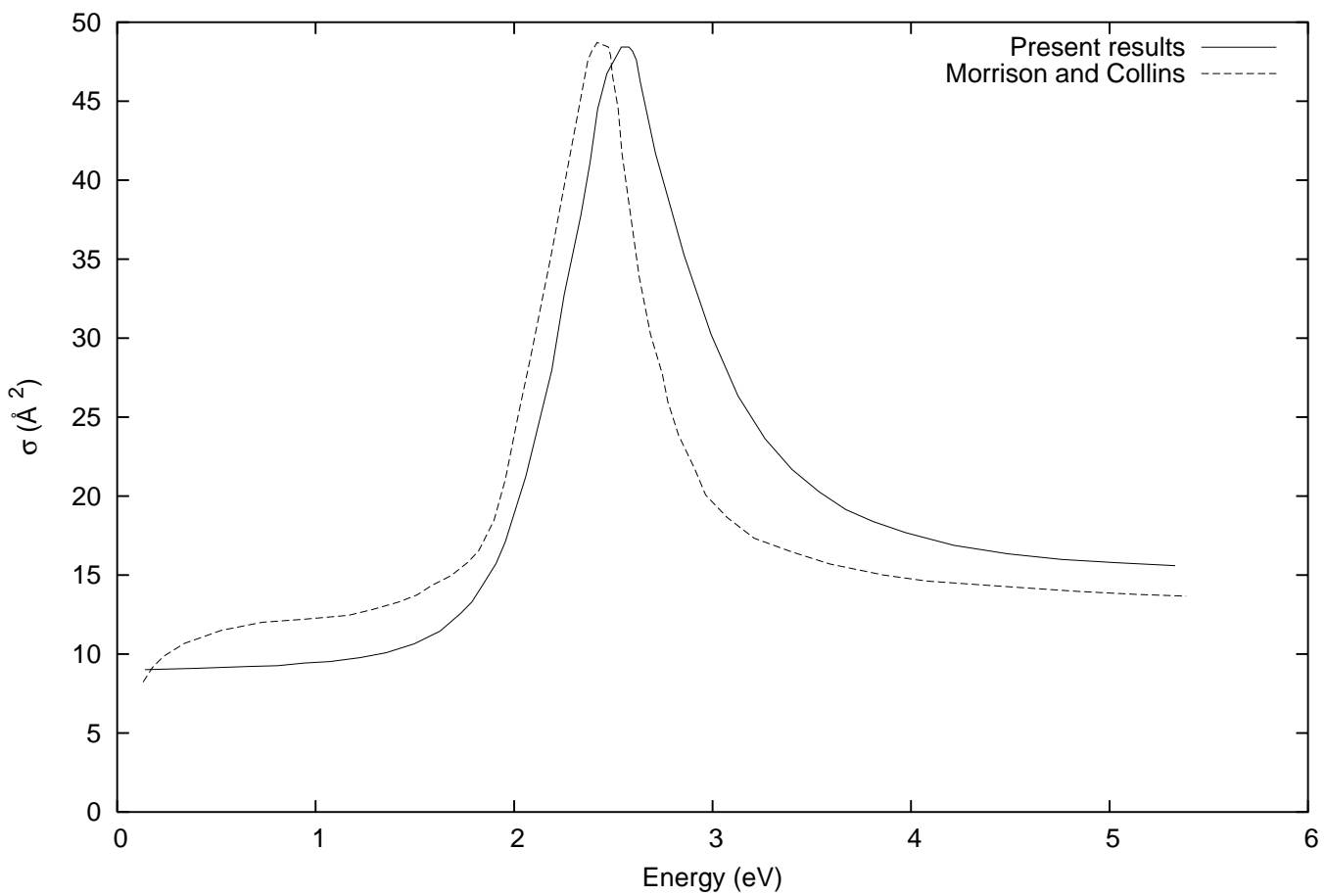


FIG. 4: Total elastic cross section for electron-N<sub>2</sub> scattering, compared to the theoretical results of Morrison and Collins. [4]

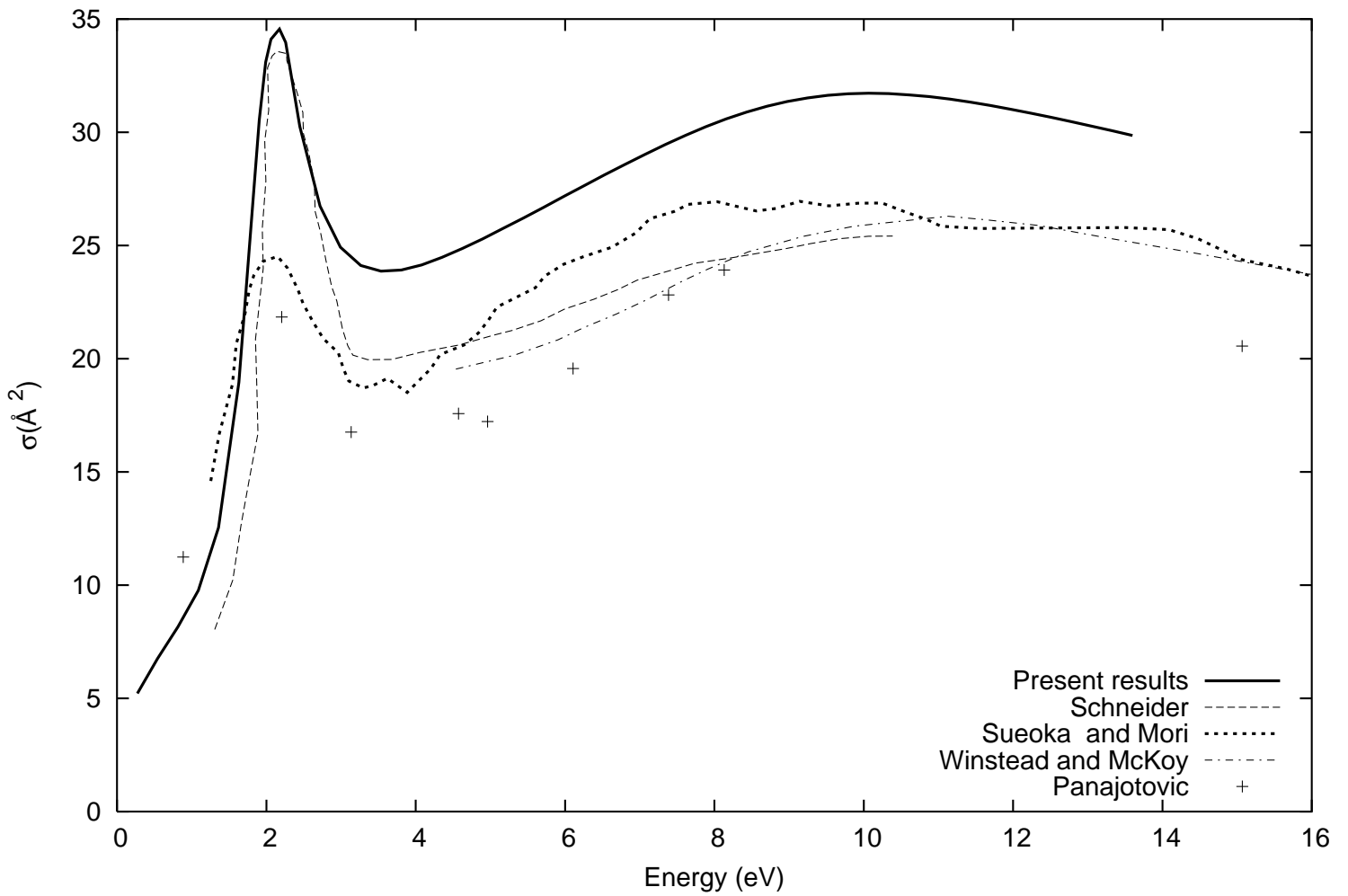


FIG. 5: Total elastic cross section for electron- $\text{C}_2\text{H}_4$  scattering, compared to previous theoretical results of Winstead *et. al.* [38] and of Schneider *et. al.* [39]. The experimental results are the ones of Panajotovic *et. al.* [40] and of Sueoka and Mori. [41]

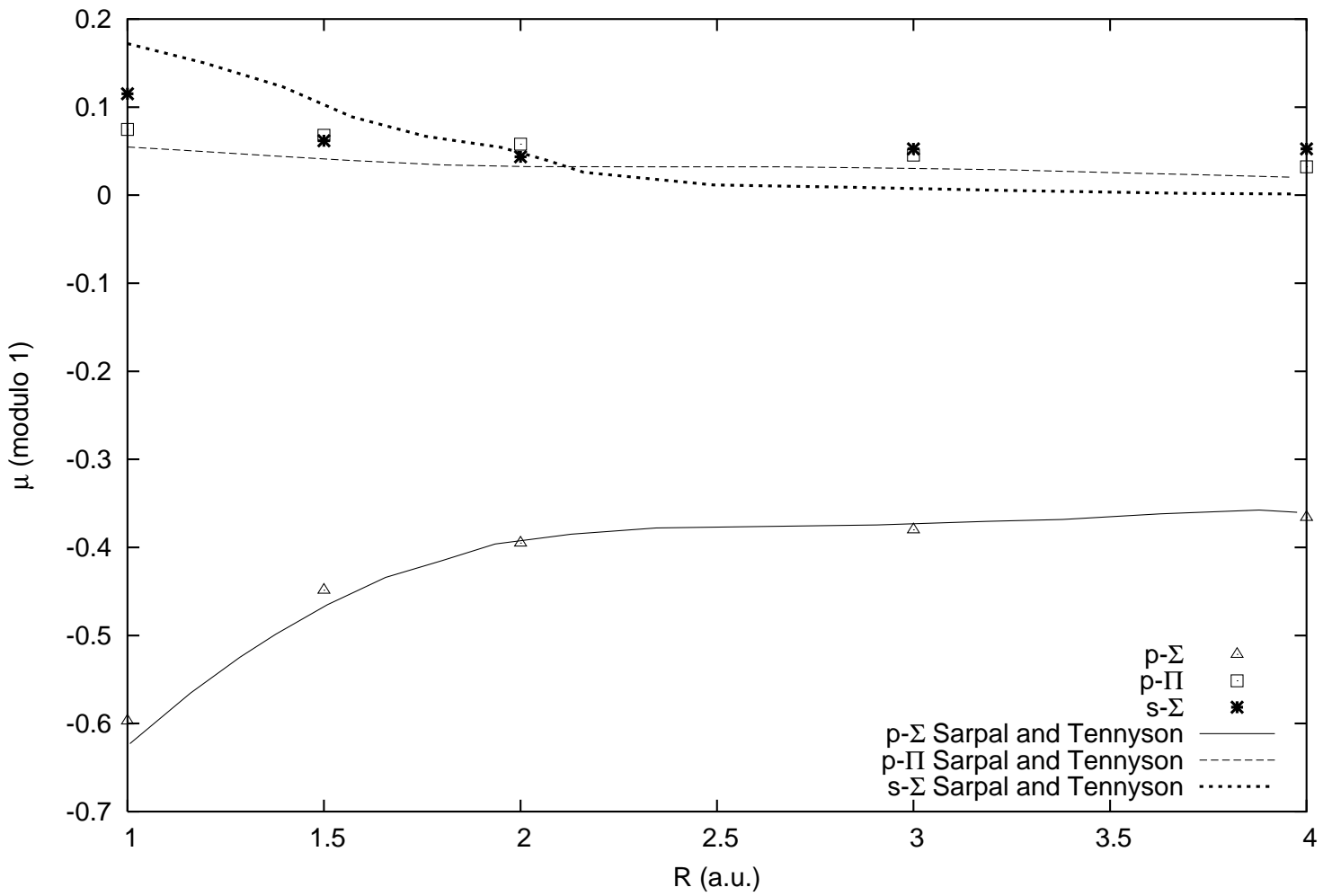


FIG. 6: Comparison of quantum defects for the HeH molecule calculated with our method to the calculations of Sarpal and Tennyson.[36]

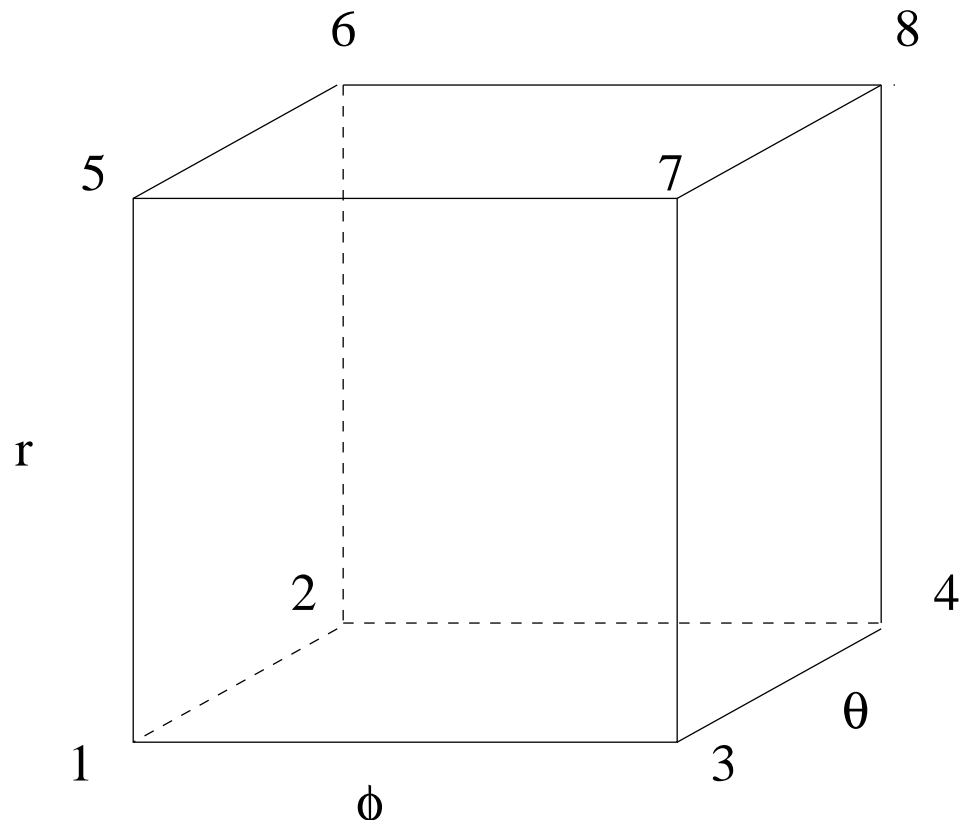


FIG. 7: Nodal structure for each finite element sector: indicated are the spherical coordinates and the numbering of the nodes at the vertices of the sector.

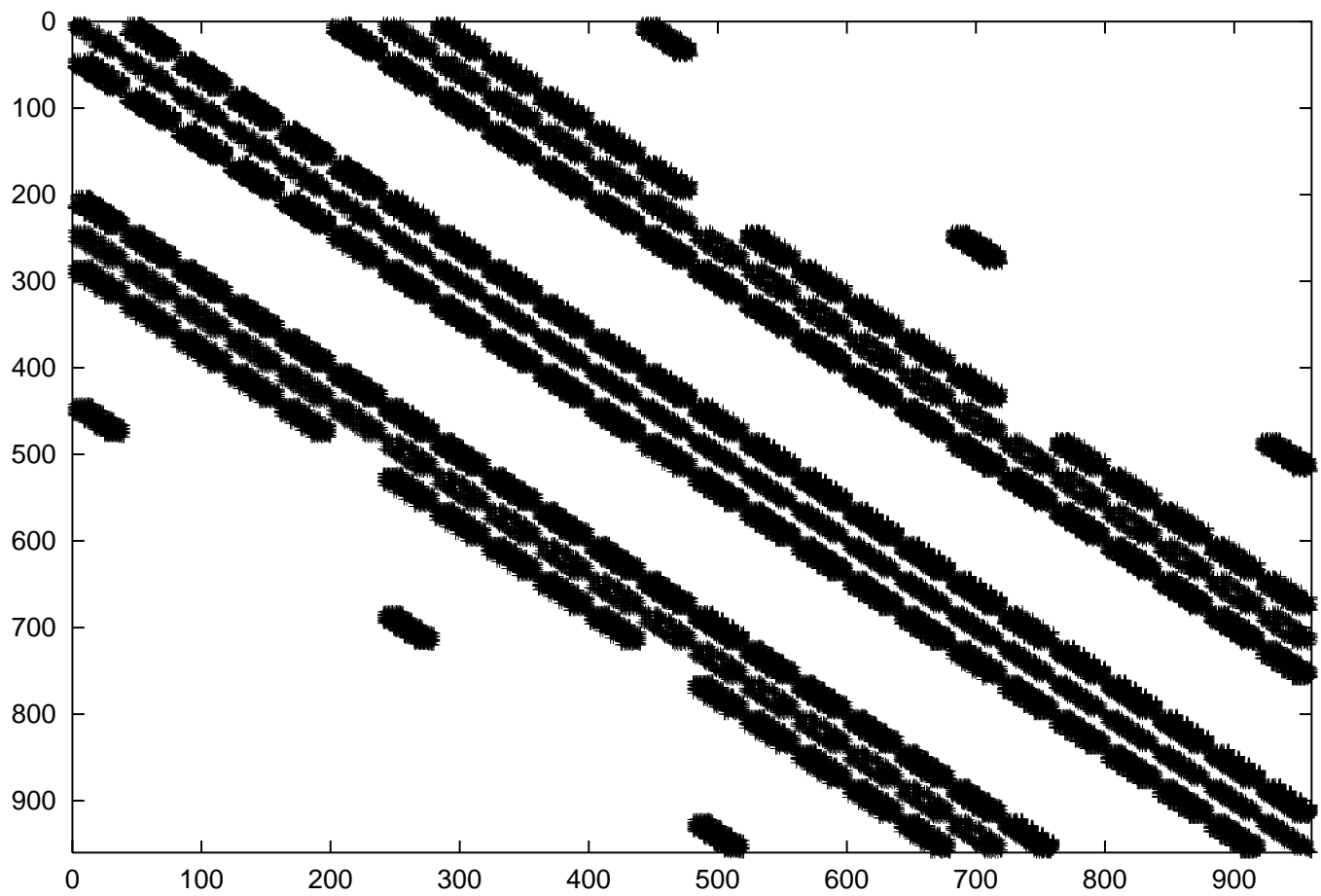


FIG. 8: Structure of the finite element matrix  $\Gamma$  for a small test case of dimension 900. It is possible to notice the great sparsity of the matrix, which increases with the dimension of the matrix.